BNL-66572

Submitted to the proceedings volume of the 1999 Joint International Meeting (196th Meeting of the Electrochemical Society and 1999 Fall meeting of the electrochemical Society of Japan with technical co-sponsorship of the Japan society of Applied Physics), October 17-22, 1999, Honolulu, Hawaii, USA.

NEW FINDINGS ON THE PHASE TRANSITIONS IN $Li_{1-X}CoO_2$ AND $Li_{1-X}NiO_2$ CATHODE MATERIALS DURING CYCLING: *IN SITU* SYNCHROTRON X-RAY DIFFRACTION STUDIES.

X. Q. Yang, X. Sun, and J. McBreen
Brookhaven National Laboratory, Upton, NY 11973

Key words: in situ XRD, cathode materials, lithium batteries.

DISCLAIMER

NEW FINDINGS ON THE PHASE TRANSITIONS IN $Li_{1-X}CoO_2$ AND $Li_{1-X}NiO_2$ CATHODE MATERIALS DURING CYCLING: *IN SITU* SYNCHROTRON X-RAY DIFFRACTION STUDIES.

X. Q. Yang, X. Sun, and J. McBreen
Brookhaven National Laboratory, Upton, NY 11973

Abstract

We have utilized synchrotron x-ray radiation to perform "in situ" x-ray diffraction studies on $Li_{1-x}CoO_2$ and $Li_{1-x}NiO_2$ cathodes. A C/10 charging rate was used for a $Li/Li_{1-x}CoO_2$ cell. For the $Li/Li_{1-x}NiO_2$ cells, C/13 and C/84 rates were applied. The in situ XRD data were collected during the first charge from 3.5 to 5.2 V. For the $Li_{1-x}CoO_2$ cathode, in the composition range of x=0 to x=0.5, a new intermediate phase H2a was observed in addition to the two expected hexagonal phases H1 and H2. In the region very close to x=0.5, some spectral signatures for the formation of a monoclinic phase M1 were also observed. Further, in the x=0.8 to x=1 region, the formation of a CdI_2 type hexagonal phase has been confirmed. However, this new phase is transformed from a $CdCl_2$ type hexagonal phase, rather than from a monoclinic phase M2 as previously reported in the literature. For the $Li_{1-x}NiO_2$ system, by taking the advantage of the high resolution in 2θ angles through the synchrotron based XRD technique, we were able to identify a two-phase coexistence region of hexagonal phase H1 and H2, which has been mistakenly indexed as a single phase region for monoclinic phase M1. Interesting similarities and differences between these two systems are also discussed.

Introduction

$LiCoO_2$ and $LiNiO_2$ with layered structures and $LiMn_2O_4$ with a cubic spinel structure are the three most widely studied cathode materials for rechargeable lithium batteries. Among these three materials, $LiCoO_2$ with a layered structure is the most widely used cathode material in commercial lithium ion batteries. On the other hand, $LiNiO_2$ and doped $LiNi_{1-y}M_yO_2$ (y=Co, Mg, Al etc.) are very attractive materials for their low cost and high capacities. X-ray diffraction (XRD) is one of the most powerful tools to study the structure of these materials. Goodenough [1,2] carried out the original studies of $LiCoO_2$ materials. The first *in situ* XRD studies during charge were published by Reimers and Dahn [3]. In the phase diagram for $0<x<0.6$ derived from that study, a monoclinic phase M1 for $0.45<x<0.55$ was reported. Ohzuku [4] published *ex situ* XRD data later and derived a phase diagram for $0<x<0.85$. In that study, a second monoclinic phase M2 was reported in $0.75<x<0.85$ region coexisting with the H2 phase. Amatucci, Tarascon, and Klein [5] published their *in situ* XRD studies for $0<x<1$ in 1996. A new phase transition, from a

monoclinic phase M2 to a CdI_2 type single-layered hexagonal phase O1 was reported for $0.9<x<1$. The "O1" nomenclature was used to reflect the CoO_6 octahedral stacking in "c" direction. O1 indicates that the unit cell in "c" direction has only one layer of octahedral. This type of stacking distinguishes this structure from the lithiated hexagonal phases (H1 and H2) in this system, which has three layers of octahedral in the unit celland could be labeled as O3 type of structures. (All of these O3 structured phases belong to rhombohedral space group $R\bar{3}m$ but indexed in a hexagonal setting.) For the $Li_{1-x}NiO_2$ system, Ohzuku [6] did pioneering *ex situ* XRD work on $Li_{1-x}NiO_2$ at different states of charge and discharge, and presented a phase diagram between x=0 to x=1. The whole range was divided into four distinct regions with three single-phase regions and one two-phase coexistence region. (A hexagonal phase H1 for $0<x<0.25$, a monoclinic phase M1 for $0.25<x<0.55$, a hexagonal phase H2 for $0.55<x<0.75$, and a two-phase coexistence region H2+H3 for $0.75<x<1$). More detailed in situ XRD studies for $Li_{1-x}NiO_2$ in the range of x=0 to x=0.82 were published by Li, Reimers, and Dahn [7]. Two more two-phase coexistence regions, H1+M1, M1+H2, were indicated and all the three phase transitions were claimed to be first order. There are three quite interesting differences in the published phase diagrams for the $Li_{1-x}CoO_2$ and $Li_{1-x}NiO_2$ systems: (1). The first phase transition in $Li_{1-x}NiO_2$ system is from H1 to M1 and the M1 phase expands in a wide range of x (from x=0.25 to 0.55). In contrast, the first phase transition in $Li_{1-x}CoO_2$ is from H1 to H2 and the M1 phase only occurs in a very narrow range (x=0.45 to 0.55). (2). The second monoclinic phase M2 was only observed in $Li_{1-x}CoO_2$ but not in $Li_{1-x}NiO_2$ system. (3). The terminal phase NiO_2 in $Li_{1-x}NiO_2$ is an O3 structured H3, while the terminal phase CoO_2 in $Li_{1-x}CoO_2$ is in O1 structure. The reasons behind these differences have not been explained in the literature. In this paper, we examine these differences by using synchrotron based in situ XRD studies. The high resolution and high signal-noise ratio of the synchrotron based technique permit us to index the Bragg reflections more accurately. Based on these results, the previously reported monoclinic phase M1 region in $Li_{1-x}NiO_2$ is reassigned to a two-phase region of H1 and H2, and the M2 region in $Li_{1-x}CoO_2$ is assigned to a two-phase region of H2 and O1.

Experimental

$Li_{1-x}NiO_2$ and $LiCoO_2$ were purchased from FMC Corp. and characterized by x-ray diffraction (XRD) using a Phillips PW1729 powder diffractometer. The lattice constants for $LiCoO_2$ are a=2.819 Å and c=14.089 Å in hexagonal setting. The lattice constants for $Li_{1-x}NiO_2$ are a=2.884 Å and c=14.216 Å. The integrated intensity ratios of $I(003)/I(104)$ were greater than 1.3 and the (108) and (110) peaks were well separated in the XRD patterns for the $LiNiO_2$. These two criteria were used in reference 6 for high quality $LiNiO_2$ material. Cathodes were prepared by slurrying $LiCoO_2$ and $Li_{1-x}NiO_2$ powder with 10% PVDF (KynarFlex 2801, Atochem), and 10% acetylene black (w/w) in a fugitive solvent, then coating the mixture onto Al foil. After vacuum drying at 100 °C for 12 hours, the electrode disks (2.8 cm^2) were punched and weighed. The cathodes were incorporated into cells with a Li foil negative electrode, a Celgard separator and a 1 M $LiPF_6$ electrolyte in a 1:1 EC:DMC solvent (LP 30 from EM Industries Inc.). Mylar windows instead of beryllium windows were used in these in situ cells. During the cycling test, an average discharge capacity of 190 mAh/g was obtained for $Li_{1-x}NiO_2$ and 150 mAh/g for $Li_{1-x}CoO_2$ in the range of 4.3 V

to 2.5 V. In situ XRD spectra were collected on beam line X18A at National Synchrotron Light Source (NSLS) at Brookhaven National Laboratory operated at an energy of 10375 eV (λ=1.195 Å). The step size for 2θ scan was 0.02 degree. The experimental setup was basically the same as described in our previous paper [8] and the XRD spectra were collected in transmission mode.

Results and Discussion

Figure 1 shows the first charging curve for the *in situ* cell with a $LiCoO_2$ cathode (23.2 mg active material) when charged at a constant current (0.7 mA, at C/10 rate) between 3.5 to 5.2 V. Quite often, when relative high rate is applied to a $LiCoO_2$ cathode during the first charge, the voltage will overshot a little at the beginning of charge. In Fig. 1, the voltage initially jumped to 4.1 V then rapidly relaxed to 3.96 V and formed three plateaus. The total charge capacity was 300 mAh/g and the discharge capacity was 230 mAh/g. The numbers corresponding to XRD scans in Fig. 2 and 3 are marked on the charging curve in Fig. 1. XRD data were collected in a range that covered reflections from the (003) to (113) Bragg peaks for the hexagonal structure. The in situ spectra are presented in Fig. 2 and Fig. 3. Scan 1 and the charging process was started simultaneously. The cell reached the 5.2 V limit and the charging process was terminated during scan 12. Each scan took about 50 minutes. Therefore, the increment of the x value in each scan is about 0.083. The missing data in scans 6, 10 and 11 was due to the unavailability of the x-ray beam. Since the charging process was continued during this period, the incomplete spectra are kept in the plot. All the in situ spectra in this paper are treated in the same manner.

The (003) is a single-fold peak. Thus every new (003) peak is a fingerprint for the formation of a new phase. Tracking the emergence and intensity changes of other new peaks in concurrence with the behavior of (003) peak help us to index these new peaks correctly. The spectra in (003) region are plotted separately in the left panel of Fig. 2. The formation of a new phase can be clearly observed in scan 2. In Fig. 2, a new peak assigned as $(003)_{H2a}$ starts to emerge at 14.46°, which is lower than the original $(003)_{H1}$ peak at 14.64°. It increases in intensity in scans 3 and 4, then decreases in intensity from scans 5 to 7 with little change in peak position. In scan 5, another new peak which we assigned as $(003)_{H2}$ begins to emerge at a lower angle than $(003)_{H2a}$. It grows in intensity, moves to a lower angles from scans 6 to 8 and reaches the lowest angle at 14.2° in scan 8. In scan 9, the $(003)_{H2}$ peak is the only one left and moves back to a slightly higher angle at 14.35°. This peak moves to an even higher angle at 14.6° and becomes very broad in scan 10. Another broad peak at 15.1° appears in the spectra during the 10th scan. We index this peak as $(001)_{O1}$ which, represents the formation of a new hexagonal phase O1 with the CdI_2 type structure. The detail description of this structure can be found in reference 5. The Miller indices for the remaining Bragg reflections of the three hexagonal phases with the $CdCl_2$ type structure are marked in the right panel of Fig. 2 covering (101) to (105) and in Fig. 3 covering (107) to (113). For the O1 phase with the CdI_2 type structure, the right panel of Fig. 2 contains (100) and (101) reflection while the (102), (110) and (111) reflections are marked in Fig. 3. The lattice constants obtained from least square refinements are listed in Table I for H1 (using data from scan 1); in Table II for H2a (using data from scan 4); in Table III for H2 (using data from scan 8); and in Table IV for O1 (using data from scan 12).

The lattice constant changes during the phase transitions can be determined by the positions of new Bragg peaks. Up to scan 8 in Fig. 2, the values of 2θ angles for the three phases are in the order of $2\theta(003)_{H2} < 2\theta(003)_{H2a} < 2\theta(003)_{H1}$. Therefore, the values of lattice constants "c" are in the order of $c_{H2} > c_{H2a} > c_{H1}$. On the other hand, "a" and "b" values experience very small changes during the transitions from H1 to H2a and from H2a to H2. This is reflected in Fig. 3 in which the position of (110) peak is almost unchanged from scans 1 to 9. Unlike the position of the (003) peak, which only reflects the change of the lattice constant "c", the positions of (10*l*) peaks reflect changes in both the "a" and "c" axes. Because of the large c/a ratio (about 4.93) of the hexagonal unit cell, the new $(101)_H$ and $(102)_H$ peaks basically follow the same track as $(110)_H$ peak, with almost no change in peak position from scans 1 to 9. With the increasing value of *l*, the effect of changes in "c" on the position of (104) and (105) becomes more prominent. However, the position changes of these two peaks during the phase transition from H1 to H2a and also from H2a to H2 are still rather small compared to the (003) peak. Finally, in Fig. 3, with the further increasing value of *l*, the (107) and (108) peaks closely follow all the changes of (003) peaks during the phase transitions. The new $(107)_{H2a}$ and $(108)_{H2a}$ peaks appear at lower angles to the $(107)_{H1}$ and $(108)_{H1}$ respectively. Also the new $(107)_{H2}$ and $(108)_{H2}$ peaks emerge at lower angles to the $(107)_{H2a}$ and $(108)_{H2a}$ peaks respectively. In scan 8, only single peaks corresponding to $(107)_{H2}$ and $(108)_{H2}$ can be seen in the spectrum, in agreement with the single $(003)_{H2}$ peak featured during scan 8 in Fig. 2.

According to references 3 and 4, a monoclinic phase M1 should be observed around x=0.5 in $Li_{1-x}CoO_2$. In scan 6 of Fig. 3, two new peaks are seen around the $(108)_{H2}$ peak. These two peaks are found on either side of the $(108)_{H2}$ peak. Similarly, two new peaks are also seen to envelope the $(113)_{H2}$ peak. These new peaks clearly indicate the formation of a monoclinic phase M1 around x=0.5 in $Li_{1-x}CoO_2$. Unfortunately, we are unable to accurately index these peaks due to the missing data in scan 6 caused by the unavailability of the x-ray beam. More detailed studies of this phase transition will be presented in future publications with high quality XRD data sets collected with position sensitive detector. According to reference 4 and 5, there is another monoclinic phase M2 located in the region of $0.75<x<0.85$. However, in Fig.3, no peak splitting can be identified in scans 9, 10, 11, and 12. All the new peaks can be indexed as Bragg reflections of an O1 phase structure. In our in situ XRD data, no signature for the presence of a monoclinic phase M2 was observed. After careful data comparison, one possible explanation is misidentification of the H2-O1 two-phase coexistence with a single M2 phase in references 4 and 5.

Figure 4 shows the first charging curve for the *in situ* cell with a $LiNiO_2$ cathode (20.7 mg active material) when charged at a constant current (0.5 mA, at C/13 rate) between 3.5 to 5.1 V. The total charge capacity was 320 mAh/g and the capacity on the subsequent discharge was 220 mAh/g. The theoretical capacity of $LiNiO_2$ is 275 mAh/g. The difference between the charge and discharge capacity might be due to the electrolyte decomposition and cathode degradation when charging voltage exceeds 4.3 V. These considerations make it difficult to determine the correct x value in $Li_{1-x}NiO_2$ just based on charge capacity. Therefore, the voltage was plotted against the charging time. The numbers corresponding to XRD scans in Fig. 5 and 6 are marked on the charging curve in Fig. 4.

The *in situ* XRD spectra are plotted in Fig. 5 and Fig. 6. Scan 1 was taken before charge and scan 14 was taken on open circuit (at 4.5 V) after the cell reached 5.1 V limit. Each scan took about 1.1 hours. The missing data in scans 9 and 10 was due to the x-ray

beam being unavailable. Three hexagonal phases (H1, H2, and H3) can be identified and Bragg peaks related to each of them are indexed in Figs. 5 and 6. From scan 2 to 6, no significant changes were recorded. This phenomenon is reproducible for all the $LiNiO_2$ cathodes when first charged at high rates. This effect can be attributed mainly to the inhibition of the nucleation of the new phase when the cell is charged at high rates. The formation of a new phase can be clearly observed through the emergence of a group of new peaks in scan 8. The phase transition proceeds in scan 9, and is finished between scan 10 and 11. According to references 6 and 7, the formation of a monoclinic phase is indicated by the splitting of the original H1 (10*l*) and (11*l*) peaks. However, no splitting of any H1 peaks was observed and no new peak appeared with a split feature. Rather than a transition from a hexagonal phase H1 to a monoclinic phase M1, as reported in reference 6 and 7, a phase transition from H1 to H2 and a two-phase coexistence region of these two phases were observed.

It can be seen from Figs. 5 and 6, that the in situ spectra have the great advantage of tracking the changes of individual peaks during charge and sorting them into different groups, with each group representing a single phase. We would like to focus on the (003) region first. The (003) is a single-fold peak with no degeneracy and therefore does not split during monoclinic phase formation. So every new (003) peak represents a new phase. Tracking the emergence and intensity changes of other new peaks in concurrence with the behavior of (003) peak help us to identify new phases. In scan 7, a small new $(003)_{H2}$ peak emerges at a lower angle (14.25°) than the original $(003)_{H1}$ peak (14.48°). It increases in intensity in scan 8 and 9, and finally becomes the dominant peak and shifts back to a higher angle at 14.32° in scan 11. (Unfortunately, no data is available in this region in scan 10.) The hexagonal structure of this of new phase can be further confirmed by the new $(10l)_{H2}$ peaks in Fig. 5 and 6. From scan 8 to 11, a group of new peaks appeared at higher angles compared to the original $(10l)_{H1}$ and $(113)_{H1}$ peaks in concurrence with the $(003)_{H2}$ peak. They emerge in scan 8, increase in intensity simultaneously with decreasing intensity of the H1 peaks in scans 9 and 10. For almost every $(10l)_{H1}$ and $(11l)_{H1}$ peak, except (107) and (108), a new peak located at a higher angle can be found. Therefore, these new (101), (102), (104), (105), (110), and (113) peaks were indexed to a hexagonal phase H2. However, no new peaks were observed near $(107)_{H1}$ and $(108)_{H1}$ peaks. This is a result of a compensation effect between the contracting "c" axis and the expanding "a" axis (and "b" axis) during the phase transition. The position of the new H2 peaks relating to the original H1 peaks is determined by the lattice constant changes during the phase transition from H1 to H2. These changes can be derived from the new positions of the $(003)_{H2}$ and $(110)_{H2}$ peaks. The lattice constant "c" in H2 is larger than in H1, because $(003)_{H2}$ is located at lower angle than $(003)_{H1}$, while "a" and "b" are smaller in H2 than in H1 because $(110)_{H2}$ is located at a higher angle than $(110)_{H1}$. The positions of (10*l*) peaks reflect changes in both the "a" and "c" axes. Because of the large c/a ratio (about 4.93) of the hexagonal unit cell, most of the new $(10l)_{H2}$ peaks primarily reflect changes in the "a" axis and following the same track as $(110)_{H2}$ peak. (peaks at 29.5° and some residues at 34.0° are Bragg peaks from the aluminum current collector.) From $(101)_{H2}$ to $(105)_{H2}$, all of these new peaks appear at higher angles to the $(10l)_{H1}$ peaks in scan 8. (The $(105)_{H2}$ peak is too weak to detect in scan 8, but appears at a higher angle than $(105)_{H1}$ in scan 10). At the same time, the peak separation between the $(10l)_{H2}$ and $(10l)_{H1}$ peaks decreases with increasing *l*; it is 0.55° for (101), 0.50° for (102), 0.40° for (104), and 0.25° for (105). This is because the contribution

from the "c" axis expansion increases with increasing *l*. Having the opposite effect on peak positions, this contribution compensates for the effect of the contraction of the "a" axis and reduces the peak separation. The effect of the contraction in "a" is almost canceled out by the expansion in "c" for the (107) and (108) peaks during the H1 to H2 transition. Therefore, only peak broadening but no new peaks were observed for (107) and (108) in scans 8 to 11. On the other hand, the $(110)_{H2}$ peak at 50.00°, which reflects the contraction in both the "a" and "b" axes, shows the largest peak separation (about 1.00°) from the $(110)_{H1}$ peak at 49.00°. The H2 to H3 phase transition can be clearly identified by the new H3 peaks in scans 11 to 14. The position of the $(003)_{H3}$ peak indicates that the lattice constant "c" is smaller in H3 than in either H1 or H2. In Fig. 6, the positions of $(110)_{H2}$ and $(110)_{H3}$ are the same. This indicates that the "a" and "b" axis remains unchanged during H2 to H3 phase transition. Therefore, all the new $(10l)_{H3}$ peaks emerge at higher angles to the $(10l)_{H2}$ peaks except the $(101)_{H3}$ peak, which remains at the same position as the $(101)_{H2}$ peak. The lattice constants obtained from least square refinements are listed in Table V for H1 (using data from scan 1); in Table VI for H2 (using data from scan 11); and in Table VII for H3 (using data from scan 14). No monoclinic phase was observed. The absence of the monoclinic phase is not due to the unique properties of this particular material. We have obtained similar results with different materials from other sources. It is very likely that the Bragg peaks indexed for a monoclinic phase in reference 6 and 7 belong to two hexagonal phases H1 and H2. Therefore, the same data sets for H1 and H2 used in table V and VI were combined together and indexed in the same way as in reference 6 for a single monoclinic structure. The results are listed in table VIII. The lattice constants obtained (a=4.913Å, b=2.804Å, c=5.092Å, ß=109.1°) are very close to those (a=4.99Å, b=2.83Å, c=5.05Å, ß=109.5°) as reported in reference 6. No effort was attempted to index the peaks in the same way as in reference 7, because no data were given for the $(104)_{H1}$ and $(108)_{H1}$ regions in reference 7.

In order to investigate the effects of the charging rate on the structural changes, the in situ XRD data were also collected at a slow charging rate of C/84. Fig. 7 shows the first charging curve for the *in situ* cell with a $LiNiO_2$ cathode (45.4 mg active material) when charged at a constant current (0.18 mA, at C/84 rate) between 3.5 to 5.1 V. The initial voltage jump disappeared and the voltage profile is almost the same as in reference 7. Near the end of charge, the fluctuation of voltage indicates the decomposition of the electrolyte at high voltage. The in situ spectra were collected continuously through the whole charging range with 0.01 degree of 2θ step-size. In Fig. 8 and Fig. 9, 11 scans (about 1.6 hours per scan) are plotted. These scans were taken in the charging range where the reported monoclinic phase supposes to form. Scans 1 to 10 were taken between the 27 to 43.5 hours of charge and scan 21 was taken between 58.5 to 60.1 hours. The first 16 scans collected from the beginning to the 26 hour of charge are not plotted, because only minor spectral changes occurred. The complete spectra of this slow charging data will be presented in a later publication. Since the phase transition from H1 to H2 was not completed in scan 10, scan 21 is also plotted in Figs. 8 and 9. The numbers corresponding to XRD scans in Figs. 8 and 9 are marked on the charging curve in Fig. 7. The Bragg peaks are indexed on scan 1 for H1 and on scan 21 for H2 respectively. In scan 21, the formation of H3 phase becomes obvious and the (003), (104) and (113) peaks of H3 phase are marked on scan 21. The nature of the phase transition is exactly the same as in Fig. 5 and 6 where C/13 rate was used. No evidence of monoclinic phase formation can be identified. Very interestingly, the

peak separation between $(003)_{H2}$ and $(003)_{H1}$ in Fig. 8 is obscured by peak broadening when a slow charging rate was used compared to the spectra in Fig. 5 where the charging rate was much faster. This might be one of the reasons that why the important $(003)_{H2}$ peak was not observed in reference 7 where the charging rate is even slower (C/100 from 3.5 to 4.3 V). In order to separate the $(003)_{H2}$ peak from the $(003)_{H1}$ peak, the step size and resolution in 2θ angle are also very important. In reference 7, the step-size of 0.05-degree was too coarse and the resolution was not sufficient to separate these two peaks. It is quite interesting that peak separation and peak shape can be changed by different charging rate. This will be addressed in a later publication with XRD data collected during second charge.

Conclusion

It is interesting to compare the similarities and differences in phase transitions during charge between $Li_{1-x}NiO_2$ and $Li_{1-x}CoO_2$ systems. In both systems, the first phase transition during charge is from H1 to H2. The H2 phase is characterized by a lattice expansion along the c-axis compared to the original H1 phase. The difference lies in how the expansion takes place in different systems. In Li_xCoO_2 system, the expansion along the c-axis occurs in two small steps; first from H1 to H2a and second from H2a to H2. In contrast, the expansion along c-axis in $Li_{1-x}NiO_2$ system occurs in a single large step from H1 to H2; i.e. the intermediate H2a phase is absent. The second major difference between the two systems with regard to the H1 to H2 transition is the change in the a-b plane. In $Li_{1-x}NiO_2$ system the "a" and "b" axes contract during the H1 to H2 phase transition. On the other hand, in the case of $Li_{1-x}CoO_2$, no significant changes in the "a" and "b" axes occur during the transition form H1 to H2a or from H2a to H2. These two differences might account for the following phenomenon: the phase transition from H1 to H2a in $Li_{1-x}CoO_2$ system starts even before less than 10% of the charge capacity is reached, while in $Li_{1-x}NiO_2$ system, the phase transition from H1 to H2 was retarded until more than 40% of the charge capacity is reached. This retardation of the phase transition for $Li_{1-x}NiO_2$ is probably due to the larger differences in unit cell dimensions between the H2 and H1. The third important difference lies in the formation of monoclinic phase M1. Clear spectral evidence of monoclinic phase formation was observed in $Li_{1-x}CoO_2$ system at a charge rate as high as C/10 from 3 V to 5.2 V. No real evidence of monoclinic phase formation was observed in the $Li_{1-x}NiO_2$ system even at charging rates as low as C/84. Another important difference is the terminal phase of the completely delithiated system. In $Li_{1-x}NiO_2$, the terminal NiO_2 (H3 phase) has the O3 type stacking, whereas in $Li_{1-x}CoO_2$, the terminal CoO_2 has the O1 structure. The main reason for these differences may lie on the migration of Ni cations, during both the synthesis and electrochemical charging processes. More detailed comparison of these two systems will be discussed in a later publication.

Acknowledgment

This work was supported by the U. S. Department of Energy Division of Materials Science of the Office of Basic Energy Sciences, and the Office of Energy Research, Laboratory Technology Research Program, Under Contract No. DE-AC02-98CH10886.

References

1. J. B. Goodenough, D. G. Wickham, and W. J. Croft, *J. Phys. Chem. Solids* **5** 107 (1958)
2. K. Mizushima, P. C. Jones, P. J. Wiseman, and J. B. Goodenough, *Mater. Res. Bull*, **15**, 783 (1980)
3. J. N. Reimers, and J. R. Dahn, *J. Electrochem. Soc.*, **139**, 2091 (1992).
4. T. Ohzuku and A. Ueda, *J. Electrochem. Soc.*, **141**, 2972 (1994).
5. G. G. Amatucci, J. M. Tarascon, and L. C. Klein, *J. Electrochem. Soc.*, **143**, 1114 (1996).
6. T. Ohzuku, A. Ueda, and M. Nagayama, *J. Electrochem. Soc.*, **140**, (1993), 1862.
7. W. Li, J. N. Reimers, and J. R. Dahn, *Solid State Ionics*, **67**, (1993), 123.
8. S. Mukerjee, T. R. Thurston, N. M. Jisrawi, X. Q. Yang, J. McBreen, M. L. Daroux, and X. K. Xing, *J. of Electrochem. Society*, **145**, 466 (1998).

Table I.
Observed and calculated d-spacing
of H1 hexagonal unit cell for $Li_{1-x}CoO_2$

(hkl)	$2\theta_{obs}$	d_{obs} (Å)	d_{calc} (Å)	δd (Å)
(003)	14.64	4.690	4.696	-0.0068
(101)	28.78	2.404	2.406	-0.0013
(102)	30.00	2.309	2.307	0.0018
(104)	34.65	2.006	2.006	0.0000
(105)	37.80	1.845	1.845	-0.0005
(107)	45.26	1.553	1.553	-0.0001
(108)	49.45	1.429	1.428	0.0002
(110)	50.15	1.410	1.410	0.0003
(113)	52.55	1.350	1.350	0.0002

$\lambda = 1.195$ Å a = 2.819 Å c = 14.089 Å

Table II.
Observed and calculated d-spacing
of H2a hexagonal unit cell for $Li_{1-x}CoO_2$

(hkl)	$2\theta_{obs}$	d_{obs} (Å)	d_{calc} (Å)	δd (Å)
(003)	14.46	4.748	4.743	0.0043
(101)	28.78	2.404	2.403	0.0008
(102)	30.00	2.309	2.307	0.0019
(104)	34.50	2.015	2.011	0.0036
(105)	37.65	1.852	1.852	0.0000
(107)	45.00	1.561	1.561	-0.0001
(108)	49.15	1.437	1.437	-0.0003
(110)	50.25	1.407	1.408	-0.0006
(113)	52.55	1.350	1.350	0.0001

$\lambda = 1.195$ Å a = 2.816 Å c = 14.230 Å

Table III.
Observed and calculated d-spacing
of H2 hexagonal unit cell for $Li_{1-x}CoO_2$

(hkl)	$2\theta_{obs}$	d_{obs} (Å)	d_{calc} (Å)	δd (Å)
(003)	14.35	4.784	4.790	-0.0061
(101)	28.78	2.404	2.402	0.0020
(102)	30.00	2.309	2.307	0.0011
(104)	34.55	2.012	2.016	-0.0044
(105)	37.62	1.853	1.858	-0.0054
(107)	44.70	1.571	1.570	-0.0007
(108)	48.80	1.446	1.446	0.0006
(110)	50.25	1.407	1.407	0.0005
(113)	52.55	1.350	1.350	0.0000

$\lambda = 1.195$ Å a = 2.813 Å c = 14.370Å

Table IV.
Observed and calculated d-spacing
of O1 hexagonal unit cell for $Li_{1-x}CoO_2$

(hkl)	$2\theta_{obs}$	d_{obs} (Å)	d_{calc} (Å)	δd (Å)
(001)	16.10	4.267	4.237	0.0301
(100)	28.25	2.448	2.449	-0.0004
(101)	32.80	2.116	2.120	-0.0039
(102)	43.80	1.602	1.602	-0.0001
(110)	50.00	1.414	1.414	0.0000
(111)	52.90	1.341	1.341	0.0004

$\lambda = 1.195$ Å a = 2.828 Å c = 4.237 Å

Table V.
Observed and calculated d-spacing
of H1 hexagonal unit cell for $Li_{1-x}NiO_2$

(hkl)	$2\theta_{obs}$	d_{obs} (Å)	d_{calc} (Å)	δd (Å)
(003)	14.48	4.741	4.739	0.0023
(101)	28.15	2.457	2.460	-0.0027
(006)	29.20	2.370	2.369	0.0010
(102)	29.40	2.355	2.356	-0.0015
(104)	34.00	2.044	2.043	0.0004
(105)	37.15	1.876	1.876	-0.0006
(107)	44.58	1.575	1.576	-0.0003
(108)	48.74	1.448	1.448	0.0002
(110)	48.95	1.442	1.442	0.0004
(113)	51.34	1.379	1.379	0.0000

$\lambda = 1.195$ Å a = 2.884 Å c = 14.216 Å

Table VI.
Observed and calculated d-spacing
of H2 hexagonal unit cell for $Li_{1-x}NiO_2$

(hkl)	$2\theta_{obs}$	d_{obs} (Å)	d_{calc} (Å)	δd (Å)
(003)	14.32	4.794	4.800	-0.0063
(101)	28.73	2.408	2.409	-0.0010
(006)				
(102)	29.90	2.316	2.314	0.0020
(104)	34.38	2.022	2.022	0.0002
(105)	37.40	1.864	1.863	0.0003
(107)	44.62	1.574	1.574	0.0002
(108)	48.70	1.449	1.449	-0.0002
(110)	50.12	1.411	1.411	-0.0003
(113)	52.38	1.354	1.354	0.0002

$\lambda = 1.195$ Å a = 2.822 Å c = 14.400 Å

Table VII.
Observed and calculated d-spacing
of H3 hexagonal unit cell for $Li_{1-x}NiO_2$

(hkl)	$2\theta_{obs}$	d_{obs} (Å)	d_{calc} (Å)	δd (Å)
(003)	15.40	4.459	4.451	0.0080
(101)	28.80	2.403	2.403	-0.0004
(006)				
(102)	30.20	2.294	2.294	-0.0005
(104)	35.28	1.972	1.971	0.0003
(105)	38.70	1.803	1.803	0.0007
(107)	46.82	1.504	1.574	0.0003
(108)	51.40	1.378	1.378	-0.0004
(110)	50.15	1.410	1.410	-0.0005
(113)	52.75	1.345	1.345	0.0005

$\lambda = 1.195$ Å a = 2.821 Å c = 13.354 Å

Table VIII.
Observed and calculated d-spacing when H1 and H2 peaks are indexed in a monoclinic unit cell as in reference 6 for $Li_{1-x}NiO_2$

(hkl)	$2\theta_{obs}$	d_{obs} (Å)	d_{calc} (Å)	δd (Å)
(001)	14.32	4.794	4.812	-0.0178
$(20\bar{1})$	28.15	2.457	2.424	0.0330
(110)	28.73	2.408	2.400	0.0083
$(11\bar{1})$	29.90	2.316	2.309	0.0066
$(20\bar{2})$	34.00	2.044	2.036	0.0073
(111)	34.38	2.022	2.016	0.0060
$(11\bar{2})$	37.40	1.864	1.864	-0.0006
(112)	44.62	1.574	1.571	0.0026
$(11\bar{3})$	48.70	1.449	1.452	-0.0027
$(31\bar{1})$	50.12	1.411	1.414	-0.0034
(310)	52.38	1.354	1.355	-0.0009

$\lambda = 1.195$ Å
a = 4.911 Å b = 2.806 Å c = 5.090 Å
ß = 109.141°

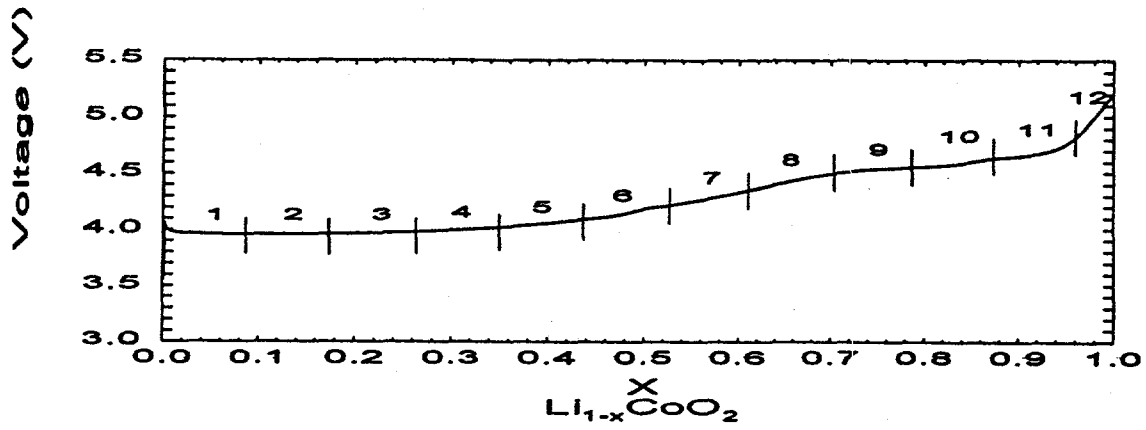

Figure 1. The first charging curve of a $Li/Li_{1-x}CoO_2$ cell at the C/10 rate from 3.5 to 5.2 V .

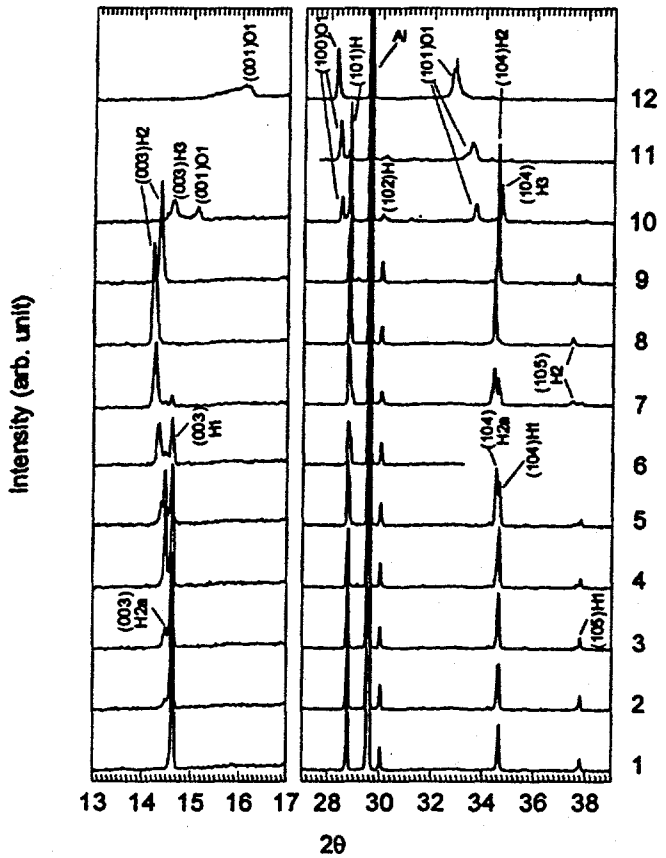

Figure 2 *In situ* XRD patterns for a $Li_{1-x}CoO_2$ cathode in the (003) to (105) region of the hexagonal structure during first charge at the C/10 rate from 3.5 to 5.2 V, 50 min for each 2θ scan from 13° to 54° (λ=1.195 Å).

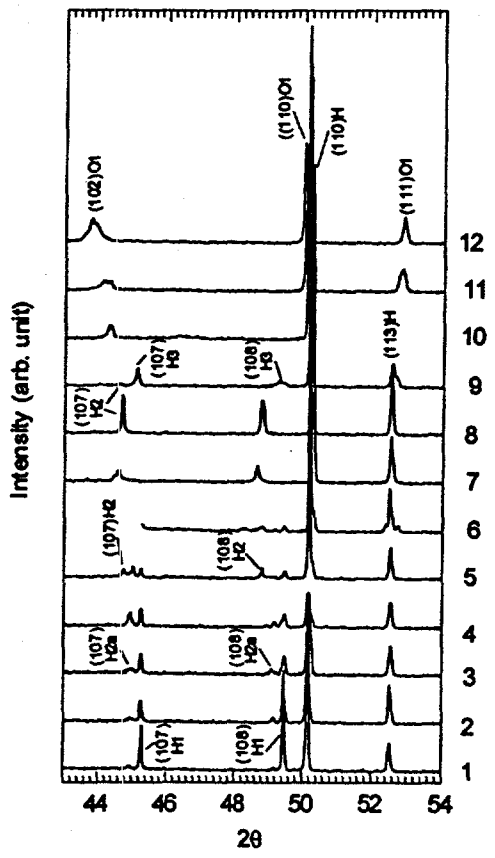

Figure 3 *In situ* XRD patterns for a $Li_{1-x}CoO_2$ cathode in the (107) to (113) region of the hexagonal structure during first charge at the C/10 rate from 3.5 to 5.2 V, 50 min for each 2θ scan from 13° to 54° (λ=1.195 Å).

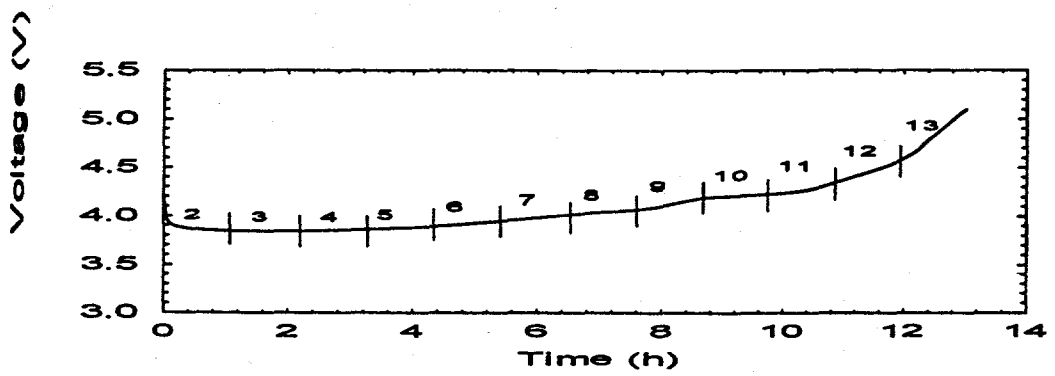

Figure 4. The first charging curve of a Li/$Li_{1-x}CNiO_2$ cell at the C/13 rate from 3.5 to 5.1 V.

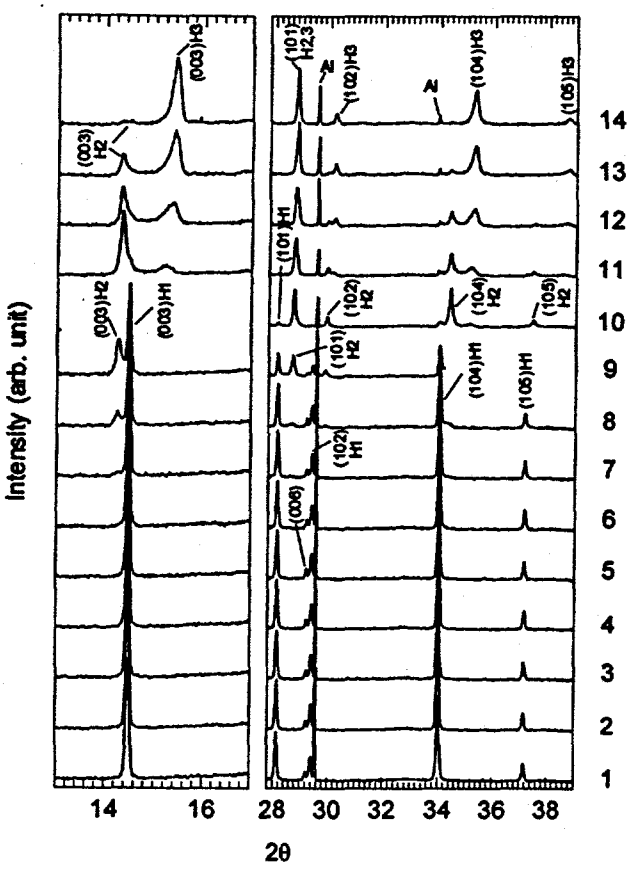

Figure 5 *In situ* XRD patterns for a $Li_{1-x}NiO_2$ cathode in the (003) to (105) region of the hexagonal structure during first charge at the C/13 rate from 3.5 to 5.1 V, 66 min for each 2θ scan from 13° to 54° (λ=1.195 Å).

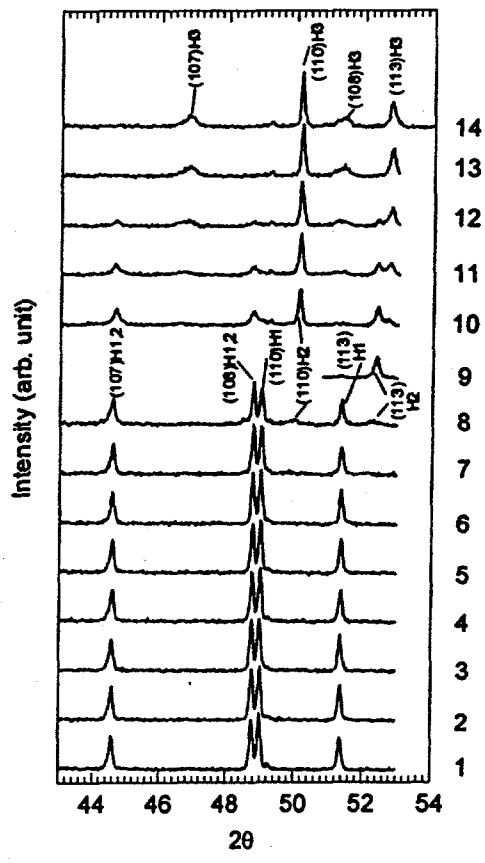

Figure 6 *In situ* XRD patterns for a $Li_{1-x}NiO_2$ cathode in the (107) to (113) region of the hexagonal structure during first charge at the C/13 rate from 3.5 to 5.1 V, 66 min for each 2θ scan from 13° to 54° (λ=1.195 Å).

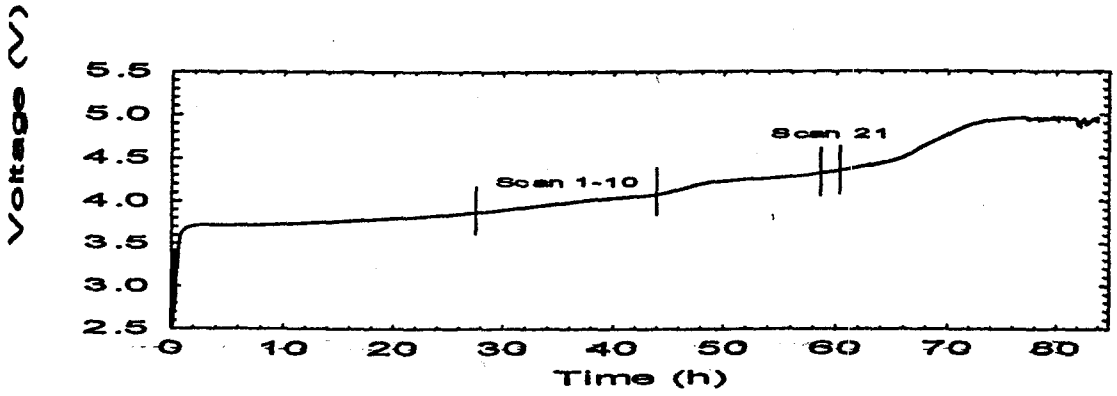

Figure 7. The first charging curve of a Li/$Li_{1-x}CNiO_2$ cell at the C/84 rate from 3.5 to 5.0 V.

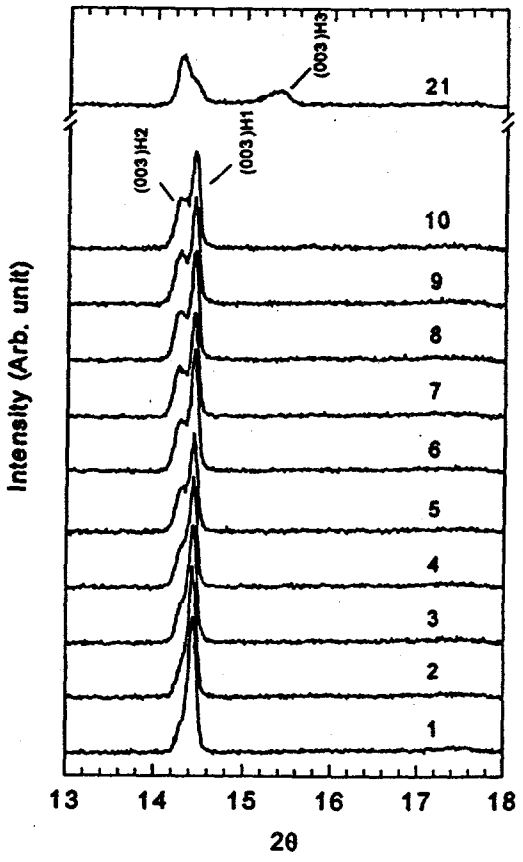

Figure 8 *In situ* XRD patterns for a $Li_{1-x}NiO_2$ cathode in the (003) region of the hexagonal structure during first charge from27 to 34.5 h and from 58.5 to 60.1 h (at the C/84 rate from 3.5 to 5.0 V) 1.65 h for each 2θ scan from 13° to 54° (λ=1.195 Å).

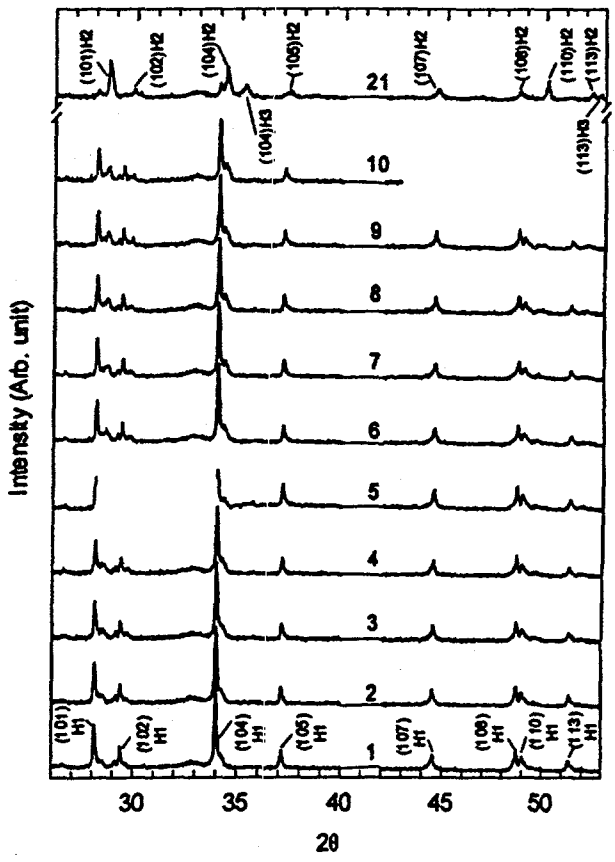

Figure 9 *In situ* XRD patterns for a $Li_{1-x}NiO_2$ cathode in the (101) to (113) region of the hexagonal structure during first charge from27 to 34.5 h and from 58.5 to 60.1 h (at the C/84 rate from 3.5 to 5.0 V) 1.65 h for each 2θ scan from 13° to 54° (λ=1.195 Å).